

# Hydrogen Welding and Hydrogen Switches in a Monatomic Gold Nanowire

Robert N. Barnett, Hannu Häkkinen,<sup>†</sup> Andrew G. Scherbakov, and Uzi Landman\*

*School of Physics, Georgia Institute of Technology, Atlanta, Georgia 30332*

*Received June 18, 2004; Revised Manuscript Received August 26, 2004*

## ABSTRACT

Ab initio density-functional calculations are performed to study the interaction between a monatomic gold nanowire suspended between two gold tips and hydrogen, in the molecular, quasi-dissociated, dissociated, and atomic forms. Structural configurations, electronic states, vibrational modes, and electronic transport are investigated for several elongation stages of the wire, corresponding to the last conductance plateau ( $G \approx 1 g_0$ ,  $g_0 = 2e^2/h$ ) before breaking of the contact. We illustrate “welding” and restoration of electric conductance of a broken wire through the incorporation of an  $H_2$  molecule, and an electric switching action resulting from structural fluctuations of an adsorbed molecule caused by mechanical forces applied to the wire.

Formation, stability, structural, and mechanical characteristics of nanowires (NWs) formed upon separation of the contact between a tip and a surface have been predicted in early simulations,<sup>1</sup> and these properties, as well as the electronic structure and electric transport in metal NWs, have been the subject of subsequent significant research efforts.<sup>2</sup> These endeavors were motivated by fundamental interest in the properties of materials contacts and wires in the nanoscale regime, as well as by prospects of using stable electrical contacts of nanoscale dimensions in future nanoelectronics.

The ultimate limit of a thin conductor is a nanowire composed of an atomic chain. Such NWs have indeed been observed in the aforementioned early simulations of gold nanowires,<sup>1</sup> as well as in the first ab initio simulations of sodium nanowires,<sup>3</sup> and more recently they have been imaged by high-resolution transmission electron microscopy (HRTEM) as a gold STM tip was retracted from gold surface.<sup>4</sup> Formation of atomic gold chains composed of several atoms has also been reported in break-junction experiments<sup>5</sup> and imaged via HRTEM as connecting bridges between areas in thin gold films perforated by impact of energetic electrons.<sup>4,6</sup> In addition to these experimental studies, the atomic and electronic structure, as well as electric conductance in such monatomic NWs, have been the focus of several theoretical investigations.<sup>7–12</sup>

While to date investigations of nanowires focused mainly on clean (bare) systems, it is natural to enquire about modifications of the mechanical, structural, and electronic properties of NWs that may be brought about as a result of their interactions with atomic and molecular species. Such

issues may be pursued from both fundamental and applied perspectives. In particular, we remark here on “nanowire chemistry” that may be viewed as an emerging topic in the broader field of nanocatalysis<sup>13,14</sup> which aims at investigations of the chemical properties and catalytic activity of systems where at least one of the dimensions has been reduced to the nanoscale. Indeed, understanding the nature of such chemical interactions may provide new avenues for chemical sensing and for catalytic applications. In the context of nanocatalysis we remark that recent research in this area focused on nanoscale gold structures, which have been found (experimentally and theoretically) to exhibit unique chemical and catalytic properties. These remarkable chemical properties of gold, which in bulk form is known to be chemically inert, have been shown to originate from the strongly modified electronic structure of gold nanoclusters and nanostructures as their size and/or dimensionality are reduced.<sup>13–15</sup>

Currently investigations of nanowires interacting with atomic or molecular species are rather scarce. Examples include (i) measurements of the electronic transport properties of nanowires in solution, prepared in an electrochemical cell;<sup>16–18</sup> (ii) an early theoretical (density-functional) investigation of structural, electronic, and transport effects of molecular adsorption on the properties of a nanowire,<sup>10</sup> in particular, bonding of methyl thiol to a monatomic gold nanowire, with implications pertaining to “anomalously” large inter-gold distances reported in some HRTEM measurements<sup>4,6</sup> [in this study<sup>10</sup> it was first suggested that the above anomaly has origins in the increased distance between neighboring gold atoms caused by interactions with a light chemical species (e.g. sulfur, carbon, hydrogen)—since the latter is essentially invisible under the imaging conditions

\* Corresponding author: email uzi.landman@physics.gatech.edu.

<sup>†</sup> Current address: Department of Physics, Nanoscience Center, University of Jyväskylä, Finland.

used for viewing the gold, its undetected presence can lead to the (erroneous) assignment of an unusually large inter-gold distance]; (iii) more recent theoretical investigations of the interactions of various elements (e.g. hydrogen, carbon, sulfur atoms), focusing on the above-mentioned “distance anomaly”;<sup>19–21</sup> and (iv) most recent experimental and theoretical investigations of the interaction of hydrogen with platinum and gold wires.<sup>22–24</sup>

In this communication we report an extensive density-functional investigation on the interaction of hydrogen with an atomic gold wire suspended between gold tips. We demonstrate a novel mechanism for the H<sub>2</sub>–wire interaction, where the hydrogen molecule can adsorb on the wire either dissociatively or molecularly depending on the stretching state of the wire. The dissociative adsorption, which is stabilized by relativistic bonding effects in gold, “switches off” the conductance of the wire, while the molecular “bridging” adsorption induces an increase in the conductance of the highly strained wire and can even restore a (fractional) conductance in a broken gold contact, with the hydrogen molecule acting as a “welding” agent. We also discuss vibrational modes of adsorbed molecular hydrogen and illustrate their sensitivity to the elongation of the nanowire.

**Computational Method.** The calculations were performed using the ab initio Born–Oppenheimer (BO) local-spin-density (LSD) molecular dynamics method (BO-LSD-MD)<sup>25</sup> including self-consistent gradient corrections (GGA)<sup>26</sup> to the exchange correlation functional. The 5d<sup>10</sup>6s<sup>1</sup> valence electrons of a gold atom are described by scalar-relativistic norm-conserving nonlocal pseudopotentials<sup>27</sup> (core radii  $s(2.5 a_0)$ ,  $p(3.0 a_0)$ ,  $d(2.0 a_0)$ , with  $s$  as the local component) using a plane-wave basis set with a kinetic energy cutoff of 62 Ry. For hydrogen, an s-only local pseudopotential with a core radius of  $0.95 a_0$  was used.

In calculations of the conductance we used a recursion transfer matrix method.<sup>28</sup> In this method the transmission of an electron propagating from one electrode to the other through the GGA self-consistent effective potential<sup>29</sup> of the connected nanowire, calculated for each of the relaxed wire configurations and processed according to the procedure described in ref 30, is evaluated using a numerical solution for the stationary states to the Schrodinger equation with scattering boundary conditions. Inside the electrodes, i.e., away from the wire/electrode contact region, the effective potential converges to a constant “jellium” value which is then used to represent the continuation of the electrodes. The solution is achieved via discretization of the Schrodinger equation in slices along the wire axis and using periodic boundary conditions in the transverse directions. Transfer-matrix recursion formalism is used to propagate the solution from one slice to the adjacent one, starting from the constant-potential region in one of the electrodes and propagating through the wire into the constant-potential region of the receiving electrode. In these conductance calculations 512 plane waves were used to achieve convergence. Transformation to nonmixing eigenchannels was performed following ref 31. The recursion transfer matrix method as currently implemented requires a local potential, so in the conductance

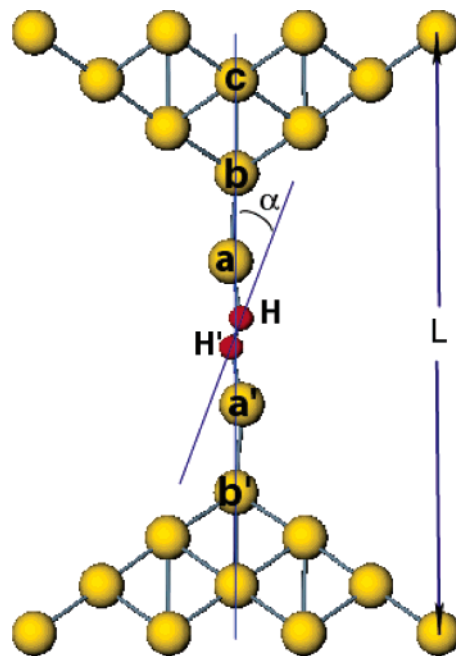


**Figure 1.** Wire setup used in the calculations; see the caption to Table 1 for the definitions of the geometric parameters.

calculations we treated Au as a 6s<sup>1</sup> valence electron atom and have solved self-consistently to get the local potential to use in the conductance calculations.

This procedure is supported by the close resemblance of the local density of states and of the wave functions on the wire atoms near the Fermi level compared to the results for the full 5d<sup>10</sup>6s<sup>1</sup> valence electron solution.

**Au Wire Setup.** Figure 1 shows the setup used in our simulations and Table 1 gives the basic parameters ( $L$ ,  $d_{aa'}$ ,  $d_{bb'}$ ,  $d_{ab}$ ,  $d_{bc}$ ) defining the bare Au wire (B wire) and the additional ones ( $\alpha$ ,  $d_{H-H'}$ ,  $d_{a-H}$ ) with the wire interacting with an H<sub>2</sub> molecule (H<sub>2</sub> wire), or with a single hydrogen atom (H wire). The parameter  $L$  gives the distance between the two outermost atomic layers of the two opposing supporting tips (with the atoms in these two layers treated statically, while all other atoms are allowed to relax dynamically after each elongation stage, i.e., when  $L$  is varied). The actual length of the monatomic wire is given by  $L_w \equiv d_{bb'}$ .

Some of the B-wire relaxed configurations that we have studied are displayed in Figure 2, and in Figure 3 we show relaxed configurations of the wire with hydrogen adsorbed. We remark that a similar setup for the bare Au wire has been used by us in a previous study of the formation mechanism of single-stranded wires from an initial double-stranded contact.<sup>12</sup> The wire system is studied here at several selected values of the stretching parameter  $L$  in the range of  $16.25 \text{ \AA} \leq L \leq 19.41 \text{ \AA}$ . The chosen lower limit of  $L = 16.25 \text{ \AA}$  corresponds to the onset of the linear monatomic wire found by us earlier for this system (for  $L < 16.25 \text{ \AA}$ , bent and zigzag configurations appear).<sup>12</sup> For each  $L$  the four atoms in the wire and the first and second layer atoms in the tips are fully relaxed.

In addition to the geometric parameters that characterize the wires, we give in Figures 2 and 3 the calculated electronic conductance ( $G$ ), the energy difference with respect to the

**Table 1.** Geometry, Energetics, and Conductance of the Wires

label <sup>a</sup>	$L^b$	$\Delta E^c$	$F_s$ (nN) <sup>d</sup>	BE(H <sub>2</sub> ) <sup>e</sup>	$G$ (g <sub>0</sub> ) <sup>f</sup>	$d_{b-b^g}$	$d_{a-a^g}$	$d_{a-H^g}$	$\alpha^h$	$d_{H-H^g}$	$d_{a-b^g}$	$d_{b-c^g}$
bare wires												
(i)	16.25	-1.24	-0.4		0.91	7.89	2.61				2.64	2.74
(ii)	17.25	-0.74	-1.4		0.87	8.51	2.79				2.86	2.93
(iii)	17.75	-0.37	-1.2		0.54	8.99	2.71				3.14	2.93
(iv md)	18.00	-0.10	-0.6		0.72	9.41	2.68				3.36	2.88
(iv ed)	18.00	-0.11	-0.1		0.05	9.44	4.19				2.62	2.89
(v)	18.25	-0.05	0.2		0.02	9.71	4.49				2.61	2.83
(vi)	18.40	-0.05	0.1		0.01	9.91	4.73				2.59	2.81
wires with H <sub>2</sub> molecule												
(vii)	16.25	-1.21	0.1	0.06	0.11	7.94	2.80	1.73	90	2.02	2.57	2.72
(viii)	17.25	-0.98	-1.2	0.32	0.07	8.51	3.05	1.75	90	1.74	2.73	2.93
(ix)	17.75	-0.77	-0.5	0.48	0.21	9.23	3.93	1.75	53	0.94	2.65	2.83
(x)	18.00	-0.78	-0.1	0.77	0.24	9.46	4.15	1.75	37	0.93	2.66	2.83
(xi)	18.25	-0.68	-0.1	0.70	0.25	9.72	4.36	1.76	19	0.94	2.68	2.84
(xii)	18.40	-0.61	-0.4	0.63	0.23	9.86	4.50	1.79	0	0.92	2.68	2.83
(xiii)	19.00	-0.30	-1.4	0.38	0.13	10.34	4.98	2.07	0	0.83	2.68	2.88
(xiv)	19.40	-0.12	-1.1	0.20	0.05	10.86	5.62	2.53	0	0.78	2.62	2.83
(d <sub>aH</sub> = 2.31)												
broken wire:		0.00	0.0	0.08	0.00	>11.2	> 6.00	2.03	0	0.78	2.60	2.81
wires with dissociated H <sub>2</sub>												
(xv)	17.25	-1.54	-1.1	0.88	0.06	8.56	2.74	1.72	0	5.62	2.91	2.91
(xvi)	18.25	-0.84	-0.2	0.88	0.09	9.63	2.71	1.72	0	6.16	3.46	2.86
(xvii)	18.40	-0.79	-0.4	0.82	0.01	9.77	2.79	1.73	0	6.26	3.49	2.87
wire with weakly bound H <sub>2</sub> molecule												
(xviii)	17.25	-0.70	-0.4	0.05	0.22	8.78	3.54	1.66	16	1.01	2.62	2.79
wire with a single H:												
(xix)	17.08		-0.6		0.00	8.54	3.37	1.69			2.59	2.82

<sup>a</sup> Labels (i), (ii), etc. identify the wire configuration and correspond to those of Figures 2 and 3, and throughout the text. <sup>b</sup> Distance (Å) between the outermost (base) atomic layers (see Figure 1). <sup>c</sup> Energy difference (eV) from a completely separated tip configuration (broken, with H<sub>2</sub> adsorbed to one tip if present). <sup>d</sup> Force of constraint (nN = 0.62 eV/Å) applied to the base layers ( $F_s < 0$  means the wire is under tension). <sup>e</sup> Energy difference (eV) from bare wire (same  $L$ ) plus H<sub>2</sub> molecule. <sup>f</sup> Conductance ( $g_0 = 2e^2/h$ ). <sup>g</sup> Distance (Å) between the specified atoms (see Figure 1). For reference we note that for the isolated hydrogen molecule  $d_{H-H} = 0.75$  Å and H<sub>2</sub> binding energy is 4.5 eV.

completely separated tips ( $\Delta E$  in Figure 2) and the H<sub>2</sub> binding energy (BE(H<sub>2</sub>) in Figure 3). These properties are also given in Table 1, and they are plotted versus elongation of the wire ( $\Delta L$  with respect to the value  $L = 16.25$  Å mentioned above) in Figure 4. Included also in Table 1 is the magnitude of the stretching force ( $F_s$ ), calculated for each equilibrated configuration (with a selected value of  $L$ ) as the force acting on the two outermost layers of the supporting tips; that is,  $F_s$  is the force required in order to maintain the given strain in the system.

**Bare Wire.** We discuss first certain properties of the bare gold wire. From inspection of Figure 4 (bottom) and Table 1 we conclude that varying the distance between the opposing tips influences mainly interatomic distances in the monatomic wire region, with the length of the wire  $L_w \equiv d_{bb'}$  increasing monotonically with  $\Delta L$ . At  $L = 18.00$  Å (i.e.,  $\Delta L = 1.75$  Å), the wire exhibits a structural bistability with two energetically degenerate configurations occurring, a middle, dimer, one (marked (iv md) in Figure 2) and an end, dimer, one (marked (iv ed) in Figure 2). For larger elongations the ed configuration dominates, resulting eventually in “breakage” of the B wire.

The structural variations of the wire are portrayed in changes in the conductance of the bare wire that is influenced only slightly when  $\Delta L = 1$  Å but drops in a step-like manner

for larger elongations (see Figure 4 top panel); note that the aforementioned bistable configurations differ greatly in conductance, with the md configurations exhibiting a much higher conductance (0.72  $g_0$ ) than the ed one. From the electrical transport point of view the contact is essentially broken for  $L \geq 18.25$  Å (see Figures 2 and 4). We also note that for  $L \geq 18.25$  Å the force required to maintain the given wire configuration changes sign; i.e., while for smaller values of  $L$  an “outward pointing” force was required in order to counterbalance the attraction between the two parts of the system, that attraction stops for  $L \geq 18.25$  Å.

**Insertion of H<sub>2</sub> into the Broken Au Contact-Welded Nanowire.** Letting the aforementioned essentially broken Au wire ( $L = 18.25$  Å,  $G = 0.02$   $g_0$ , marked (v) in Figure 2 and Table 1) interact with a hydrogen molecule results in a barrierless insertion of the molecule into the contact with a significant binding energy BE(H<sub>2</sub>) = 0.70 eV ((xi) in Figure 3 and Table 1). Concomitantly, the conductance of the “welded” contact increases from close to zero to  $G = 0.25$   $g_0$ , indicating partial opening of one conductance channel; see our remark in ref 23 pertaining to differences between the calculated conductance and that measured in experiments on physisorbed H<sub>2</sub> at 10–30 K. At this value of  $L$  the H<sub>2</sub> molecule is slightly tipped, and further stretching allows it

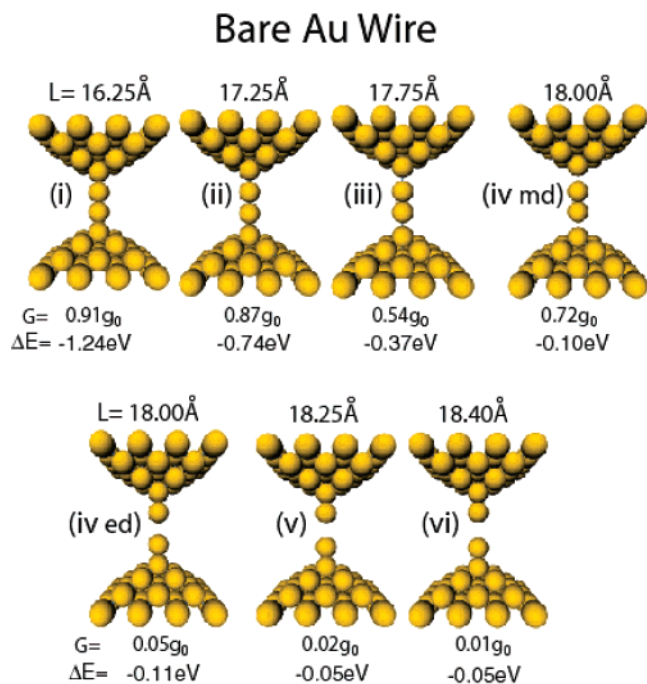


**Figure 2.** Optimal configurations of bare wires. The labels (i), (ii), etc. correspond to the first column of Table 1. For  $L = 18.00$  Å, two nearly degenerate configurations are shown, with middle-dimer (iv md) and end-dimer (iv ed) structures. For each configuration we also give the conductance ( $G$ ), and the total energy difference ( $\Delta E$ ) between the given configuration and the two separated tips.

to straighten. For  $L$  larger than  $19.40$  Å ( $L_w = 10.86$  Å), the conductance essentially vanishes and the wire is finally broken.

A barrierless insertion of the  $H_2$  molecule occurs also for  $L = 18.0$  Å (recall the bistable B wire mentioned above). Here the molecule is more strongly tilted with respect to the wire axis, and the binding energy to the wire is peaked at  $0.77$  eV (see Figure 4, middle panel, and configuration (x) in Table 1). As seen in Figure 3(x), the adsorption of the hydrogen molecule is accompanied by stabilization of the “end-dimer-like” configuration, with a relatively high conductance  $G = 0.24 g_0$  (see Figure 4, top panel). Elongation of the wire for  $L > 18.25$  Å ( $L_w > 9.72$  Å, see Table 1) results in smaller binding energies of to the wire and decreasing conductance. We note that the incorporation of the hydrogen molecule in the wire allows the wire to extend to larger lengths than the bare Au wire (see in particular the bottom panel of Figure 4).

When instead of elongating the wire it is compressed (starting from the welded configuration at  $L = 18$  Å), the tilt angle the adsorbed molecule increases and the binding energy to the wire decreases sharply (see Figure 3, middle panel of Figure 4 and (ix) in Table 1). From the bottom panel of Figure 4 we observe that the length of the wire  $L_w \equiv d_{bb'}$  as a function of the elongation  $\Delta L$  is the same for the bare wire and the one with the adsorbed hydrogen. This is due to the fact that the adsorption of the molecule results in rearrangement of the gold atoms in the internal part of the wire (see  $d_{aa'}$  in the bottom panel of Figure 4), with the two

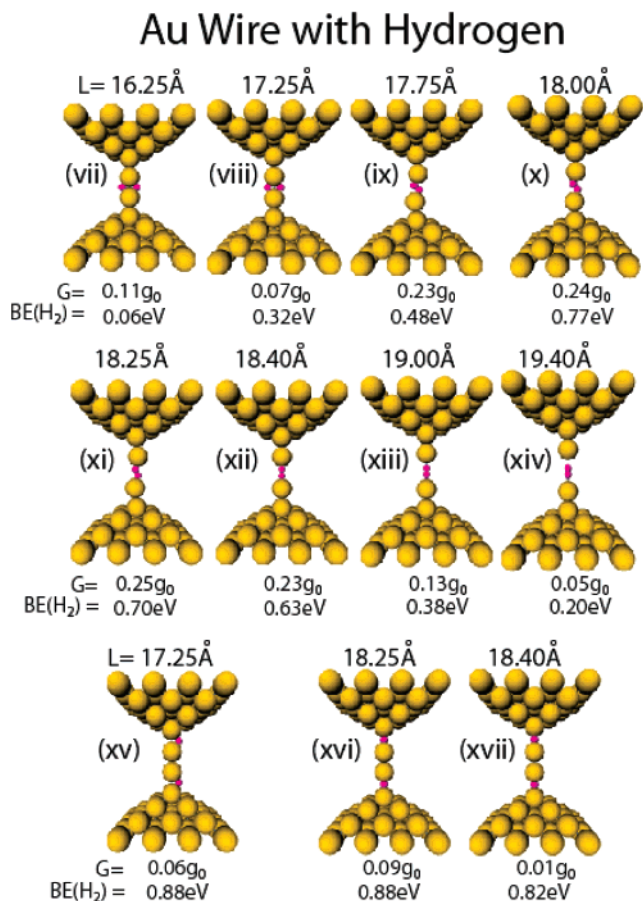


**Figure 3.** Gold wires with adsorbed hydrogen (small red spheres). Configurations (vii) and (viii) are quasi-dissociated; for larger  $L$  the adsorbed hydrogen molecules exhibit an increasing tilt angle with respect to the wire axis; (xiv) corresponds to an essentially broken wire. Hydride-wire configurations are shown in the bottom row.  $G$  is the conductance and  $BE(H_2)$  is the energy difference between the given configuration and the bare wire plus  $H_2$  molecule.

end atoms that connect the wire to the two tips remaining at almost constant distance from the respective first (4-atom) layer of the supporting tip. Finally we remark that at a short distance  $L = 17.25$  Å we found that  $H_2$  binds molecularly to the side of the wire (configuration (xviii) in Table 1, and in Figure 7 below) with a binding energy  $BE(H_2) = 0.05$  eV and a conductance  $G = 0.22 g_0$  that is a little less than half that of the corresponding B wire (configuration (ii) in Table 1 and Figure 2). The barrier to remove the  $H_2$  molecule starting from the latter equilibrium configuration reaches a maximum of about  $0.4$  eV at a radial distance of  $1.6$  Å from the wire axis (determined by minimizing energy with constrained distance from the wire axis to the  $H_2$  center of mass). The  $H_2$  molecule did not bind to the side of shorter wires.

**$H_2$  Quasi-Dissociation and the “Hydrogen Switch”.** Compression of the wire from  $L = 18.25$  Å to  $L = 17.25$ , and further to  $16.25$  Å, results in quasi-dissociation of the molecule, with the H–H axis perpendicular to the wire axis;  $d_{H-H} = 1.74$  Å and  $BE(H_2) = 0.32$  eV for  $L = 17.25$  Å and  $d_{H-H} = 2.02$  Å and  $BE(H_2) = 0.06$  eV for  $L = 16.25$  Å; see configurations (viii) and (vii) in Figure 3 and Table 1,

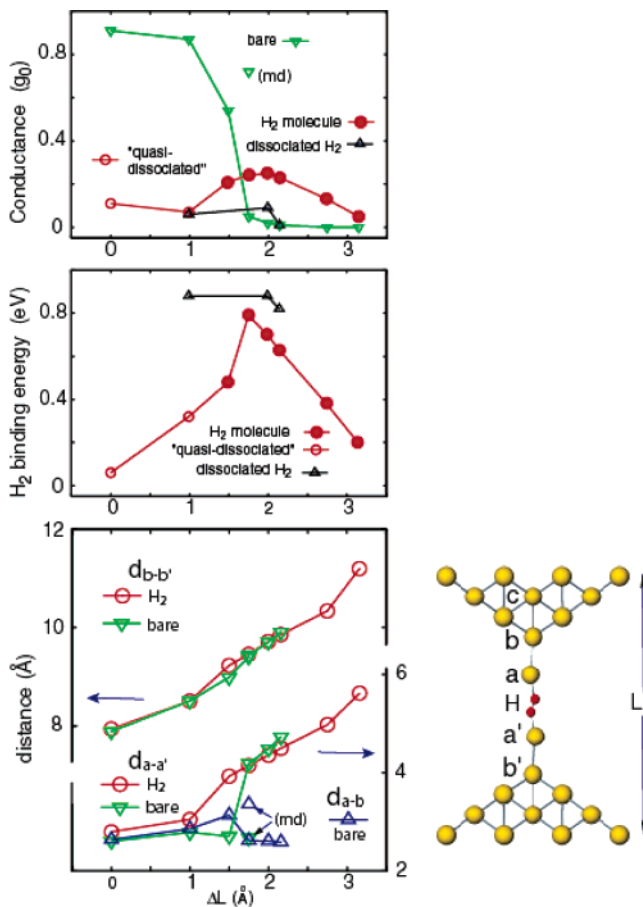


**Figure 4.** Conductance in units of  $g_0$  (top panel), the hydrogen binding energy  $BE(H_2)$  in eV (middle panel), and the variation of various distances (in Å), plotted versus the elongation  $\Delta L = L - L_0$ ,  $L_0 = 16.25$  Å (see also Table 1). The meaning of the various symbols is indicated in the figure. The “quasi-dissociated” configurations are those shown in the top row of Figure 3 ((vii) and (viii)), and the dissociated configurations are those shown in the bottom row in Figure 3 (i.e., the hydride states, labeled (xv), (xvi), and (xvii)). For  $\Delta L = 1.75$  Å, we show (for the bare wire) in the top and bottom panels results for two nearly degenerate configurations: a “middle-dimer” (md) and an “end-dimer” (ed). Only the md is marked.

respectively. The binding energies of the quasi-dissociated molecule to the wire in these compressed states are lower than the starting welded configuration (see middle panel in Figure 4). While the quasi-dissociation of H<sub>2</sub> upon compression is barrierless, a rather high activation barrier is encountered (larger than 0.8 eV) for recombination of the H atoms and removal of the H<sub>2</sub> molecule from the wire at  $L = 17.25$  Å. This indicates that once the quasi-dissociated state of the molecule has been formed it is stable and subsequently it may lead to the appearance of “hydride states” (see below).

Bonding of H<sub>2</sub> to the Au-wire has been analyzed by projecting the electron local density of states (LDOS) onto the hydrogen atoms and the neighboring Au atoms on the wire axis (labeled in Figure 1 as a, a', b, b', c). These LDOS are shown in Figure 5a and 5b, respectively, for the quasi-dissociated molecule at  $L = 17.25$  Å (viii) and for the bridging molecule case at  $L = 18.4$  Å (xii). We also include in Figure 5c the projected LDOS for a Au wire with an

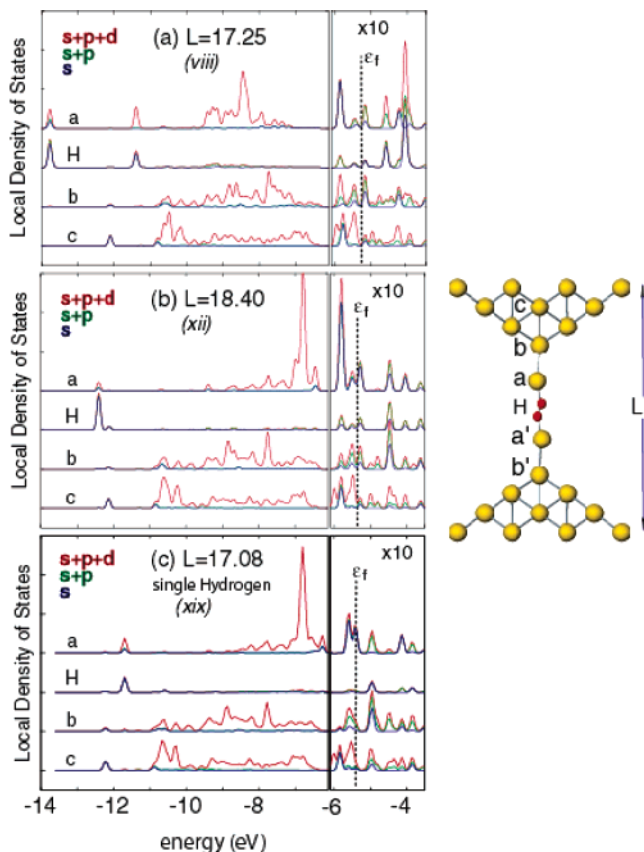


**Figure 5.** Local density of states (LDOS) for the optimal configurations of a gold nanowire with adsorbed hydrogen, corresponding to (a)  $L = 17.25$  Å (a quasi-dissociated molecule), and (b)  $L = 18.40$  Å (a hydrogen molecule inserted into the wire). The LDOS for a gold wire with an adsorbed single hydrogen atom is shown in (c). These LDOS plots were calculated using a sphere of radius 1.6 Å centered on the Au atoms (labeled a, b, and c, see Figure 1) or of radius 1.3 Å centered on the H atoms. The LDOS is decomposed into s, p, and d components: the blue curve is the s component, the green is the sum of s and p components, and the red is the sum of s, p, and d components. There is a gap below about  $-6.2$  eV, and the LDOS for energy above this gap is shown multiplied by a factor of 10.

embedded single hydrogen atom (configuration (xix) in Table 1). In Figure 6 we display isosurfaces corresponding to several wave functions near the Fermi level for the three systems shown in Figure 5.

For the bridging-molecule (Figure 5b, only one major peak in the LDOS of the hydrogen atoms is seen (located at  $-12.4$  eV in Figure 5b) and it corresponds to the lowest occupied molecular orbital (LOMO, see Figure 6) of the entire system (tips, wire, and hydrogens), located about 7 eV below the Fermi energy  $E_F$ . This state is found to be a superposition of the  $\sigma(H_2)$  bonding molecular orbital and the 5d ( $m = 0$ ) states of the Au atoms of the wire axis, creating a bonding state that extends along the wire axis. The antibonding state of the bridging molecule is unoccupied and it lies outside the energy interval shown in the figure.

For the quasi-dissociated molecule (Figure 5a) in addition to the LOMO state (located at about  $-13.9$  eV) another state is found below the gold d-band that has a large amplitude on the H atoms (marked as LOMO+3 in Figure 6a, with an

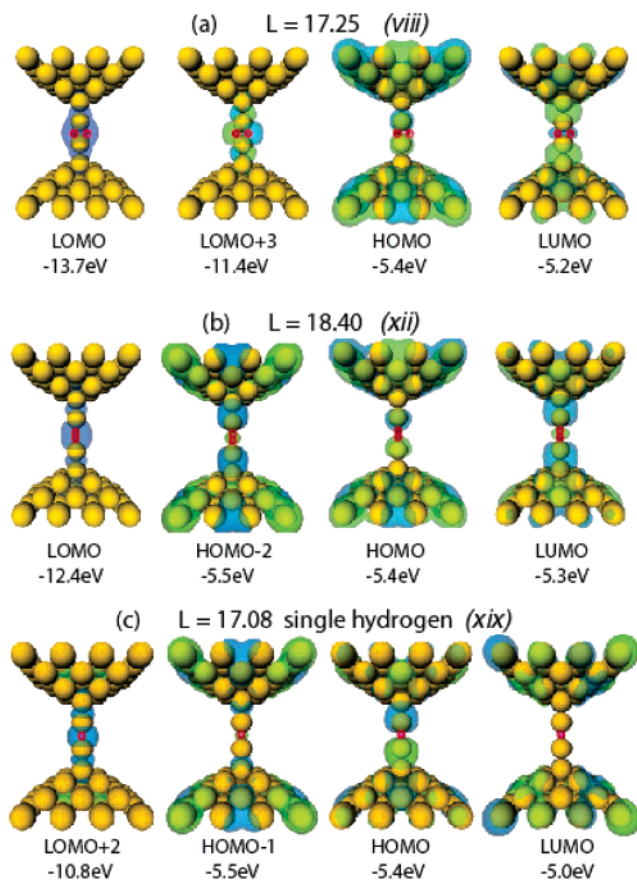


**Figure 6.** Wave function isosurfaces for the quasi-dissociated (a) and bridging-molecule (b) cases, configurations (viii) and (xii), respectively, in Figure 3 and Table 1. The LDOS for a wire with single adsorbed hydrogen atom (configuration (xix) in Table 1) is shown in (c). In these plots, LOMO is the “lowest-occupied” state, which is predominately the  $H_2$  binding orbital in case (a) and (b). HOMO and LUMO are the “highest-occupied” and “lowest-unoccupied” states. Also shown are the “LOMO+3” wave function for the quasi-dissociated case(a), which is largely the  $H_2$  antibonding orbital (a similar state is not found for the bridging-molecule configuration since the antibonding state lies above the energy interval shown here), and the “HOMO-2” for the bridging-molecule case shown in (b) (corresponding to the large peak in the LDOS of the Au atoms adjacent to the  $H_2$ ). The isosurfaces include 95% of the orbital; the green and blue correspond to positive and negative values, separated by nodal surfaces.

energy of about  $-11.7$  eV). This state corresponds to the antibonding  $\sigma^*(H_2)$  orbital that is mixed with the Au 5d states. We note that in both cases the highest occupied state (HOMO in Figure 6a,b) and lowest unoccupied (LUMO in Figure 6a,b) are delocalized over the entire system, with the LUMO showing features of the bonding  $\sigma(H_2)$  state and the HOMO showing features of the antibonding  $\sigma^*(H_2)$  state, and both are hybridized with the 6s state of the neighboring Au atoms in the wire region (the atoms labeled (a) and (a') in Figure 1). We also note here that for the single adsorbed hydrogen atom the hydrogen 1s orbital hybridizes with a 5d orbital of the neighboring gold atom (see the state at  $-11.6$  eV in Figure 5c). We note, however, that the LDOS on the hydrogen atom vanishes at the Fermi level, and the LUMO orbital has no amplitude on the wire atoms and the hydrogen atom (see Figure 6 bottom row).

The fact that the  $H_2$  molecule interacts so strongly with the gold wire is quite surprising in light of the well documented inertness of gold surfaces toward adsorption and/or promotion of dissociative  $H_2$  adsorption. However, early experiments of the reactions of neutral gas-phase coinage metal dimers indicated that among  $Cu_2$ ,  $Ag_2$ , and  $Au_2$ , the gold dimer is the only one that interacts with  $H_2$ ; additionally, these experiments indicated a slow pressure-independent rate constant and insertion of gold into the H–H bond.<sup>32</sup>

To further investigate these points, we performed comparative calculations for a free linear four-atom cluster  $Au_4$  with  $H_2$  adsorbed in the middle (that is between the second and third gold atoms, with the axis of the quasi-dissociated hydrogen molecule perpendicular to the axis of the straight gold wire), and found that depending on the nature of the gold pseudopotential (scalar-relativistic (SR) or nonrelativistic (NR)) the interaction energy is either binding (by 1.07 eV) for the SR  $Au_4$  or nonbinding for the NR gold quadramere cluster. Analysis of the local density of electronic states projected on the H atom reveals that the tendency for the SR  $Au_4$  wire to dissociatively bind  $H_2$  is due to the strong bonding overlap of the antibonding  $\sigma^*(H_2)$  state with one of the d ( $m = \pm 1$ , Au) states. As a result of the promotion of charge to the antibonding  $H_2$   $\sigma^*$  state, the  $\epsilon(\sigma^*) - \epsilon(\sigma)$  energy gap is only about 2.5 eV, whereas in the free  $H_2$  molecule it is calculated to have a 4-fold larger value of 10.2 eV. A similar scenario is observed for the suspended  $H_2$  wire with  $L = 16.25$  Å and  $L = 17.25$  Å; see Figure 5 for the LDOS and Figure 6 for the corresponding wave function portraits, with the bonding LOMO,  $\sigma(H_2)$ , and the antibonding (LOMO+3),  $\sigma^*(H_2)$ , found to be localized in the four-atom region between the tips. To our knowledge this is the first time that the tendency of an Au wire to promote dissociative adsorption of  $H_2$  is predicted and correlated to the relativistic bonding effects in gold.

The states of the wire with the adsorbed quasi-dissociated  $H_2$  molecules exhibit highly reduced conductances compared to those of the corresponding bare wire configurations (Table 1, Figure 4); at both  $L = 17.25$  and  $16.25$  Å the decrease is about  $0.8 g_0$ . Isosurfaces of the calculated conductance eigenchannels (i.e., the vectors that diagonalize the transmission matrix, expressing the probability density for transmission) of several of the B and  $H_2$  wires (both conducting and nonconducting), are shown in Figure 7. We observe that while for the B wire ((ii) for  $L = 17.25$  Å in Figure 7) the conductance eigenchannel is spread rather uniformly over the entire system (tips and connecting nanowire constriction), the hydrogen atoms in the  $H_2$  wire induce backscattering regions (regions with near vanishing probability density for transmission) for electrons in both of the tips and between the Au atoms in the wire marked (a) and the guest hydrogen atoms. This surprising theoretical prediction of the “hydrogen switch” effect could, in principle, be tested in well-controlled tip–surface experiments in hydrogen atmosphere.

**Dynamical Characteristics of the  $H_2$ -Bridged Gold Contact.** The adsorbed  $H_2$  in the Au wire remains molecular within the stretch region of  $18.25 \leq L \leq 19.40$  Å (for larger values of  $L$  the wire is considered broken), with a maximum

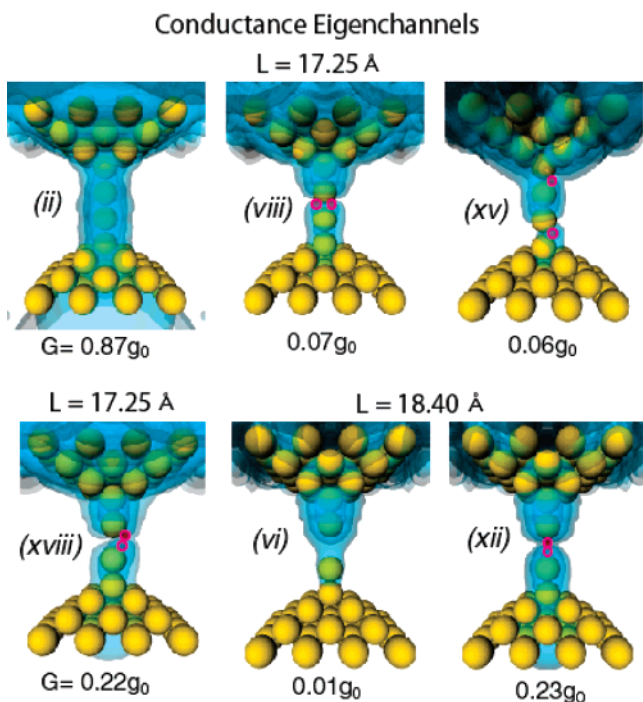


**Figure 7.** Isosurfaces of the conductance eigenchannel density for several of the wire configurations. For  $L = 17.25 \text{ \AA}$  we display results for the bare wire (ii), the quasi-dissociated state (viii), the hydride state (xv), and the weakly bound state (xviii). For  $L = 18.40 \text{ \AA}$  we display results for the bare wire (vi) and the welded one (xii). The three nested isosurfaces correspond to 10%, 1%, and 0.1%.

of  $\text{H}_2$  binding energy and conductance ( $0.70 \text{ eV}$  and  $0.25 g_0$ , respectively) at  $L = 18.25 \text{ \AA}$ . The dynamical properties of the  $\text{H}_2$ -bridged contact can be characterized by three  $\text{H}_2$  vibration modes: a “shuttle motion” (vibration of the center of mass of the molecule along the Au-wire axis) with a frequency  $\omega_1$ , a “wobble motion” (variations of the angle  $\alpha$ ) with a frequency  $\omega_2$ , and the H–H bond stretch characterized by  $\omega_3$ . We have determined the frequencies of these normal modes by ab initio molecular dynamics simulations at three stretching states with  $L = 17.25, 18.40,$  and  $19.00 \text{ \AA}$  (see Figure 8). At  $L = 17.25 \text{ \AA}$ ,  $h\omega_1 = 148 \text{ meV}$ ,  $h\omega_2 = 104 \text{ meV}$ , and  $h\omega_3 = 205 \text{ meV}$ . At  $L = 18.40 \text{ \AA}$ ,  $h\omega_1 = 130 \text{ meV}$ ,  $h\omega_2 = 58 \text{ meV}$ , and  $h\omega_3 = 308 \text{ meV}$ . At  $L = 19.0 \text{ \AA}$ ,  $h\omega_1$  decreases strongly to  $64 \text{ meV}$ ,  $h\omega_2 = 71 \text{ meV}$ , and  $h\omega_3$  is slightly reduced to  $292 \text{ meV}$ . We note here that recent scanning tunneling spectroscopy (STS) measurements, performed for a break-junction Pt atomic contact in  $\text{H}_2$  atmosphere, yielded a typical resonance frequency of about  $60 \text{ meV}$ , which was attributed to the “shuttle” motion of a bridging  $\text{H}_2$  molecule across the Pt atom contact.<sup>22</sup> Our results illustrate the marked sensitivity of the vibrational frequencies of the molecule on the stretching state of the wire. Furthermore, we observe that, depending on the state of elongation, either a “wobble” motion of the molecule (see  $L = 18.40 \text{ \AA}$  in Figure 8) or both “shuttle” and “wobble” vibrations (see  $L = 19.00 \text{ \AA}$  in Figure 8) may contribute to the observation of a phonon frequencies close to  $60 \text{ meV}$ ; in this context see our remark in ref 22.

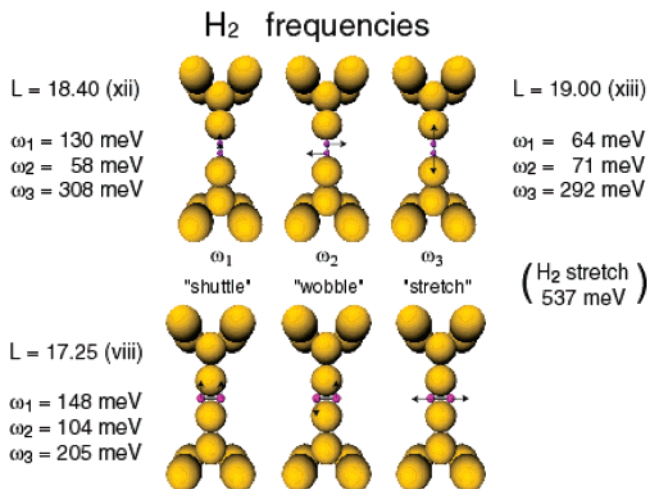


**Figure 8.** Vibrational modes of a hydrogen molecule adsorbed to a gold monatomic wire suspended between two supporting tips, calculated for different values of the intertip distance. The displacement vectors of the hydrogens corresponding to the various modes (shuttle, wobble, and stretch vibrations) are shown for  $L = 18.40 \text{ \AA}$  and  $L = 17.25 \text{ \AA}$ ; the displacement vector for the configuration with  $L = 19.00 \text{ \AA}$  have the same character as those shown for  $L = 18.40 \text{ \AA}$ .

**Gold-Hydride Wire.** As indicated above, the dissociation of the  $\text{H}_2$  molecule inside the wire may lead to other arrangements of Au and H atoms, such as the ones depicted in Figure 3(xv)–(xvii). These “hydride” wires, characterized by linear or “zigzag” alternating  $-\text{Au}-\text{H}-\text{Au}-$  chains, could be formed for example by H atom diffusion after the dissociation of an  $\text{H}_2$  molecule or via diffusion from the tips to the wire region. We have not studied these mechanisms (and the barriers involved) in more detail, but we note here that the hydride wires are remarkably stable, in agreement with a recent computational study<sup>24</sup> (in fact, their total energies are the lowest ones in the stretching region of  $17.25 \text{ \AA} \leq L \leq 18.4 \text{ \AA}$ , see Table 1). However, we find that the calculated conductance properties of the hydride wires are remarkably different from what was conjectured previously: while in ref 21 an estimate of  $G \approx 1 g_0$  was made on the basis of the calculated band structure of an infinite  $-\text{Au}-\text{H}-\text{Au}-\text{H}-$  wire, our explicit calculations on the transmission properties through the hydride wire and the tip regions indicate that the hydrogen atoms generate a significant backscattering of the electrons, and  $G < 0.1 g_0$  for all the cases that we studied here ( $L = 17.25, 18.25,$  and  $18.4 \text{ \AA}$ ). The eigenchannel for the hydride wire at  $L = 17.25 \text{ \AA}$  is shown in Figure 7(xv). We also tried a single H between the two center gold atoms of an  $L = 17.08 \text{ \AA}$  wire and found the conductance to be zero.

**Summary.** In this study we explored through extensive electronic structure calculations based on density functional theory, the energetics, structures, electronic states, and electrical conductance of: (i) bare gold nanowires made of a monatomic chain suspended between two supporting tips, and (ii) these wires interacting with hydrogen. Our calculations revealed that the interaction between a hydrogen molecule and a suspended monatomic gold wire, and the optimal outcome of such interaction, exhibit a strong

dependence on the elongation stage of the wire (occurring as a result of the displacement of the tips with respect to each other, thus straining the wire), and in some cases the interacting system may evolve along several alternative pathways.

The processes that we explored includes: (i) “molecular welding”, where a hydrogen molecule adsorbs to the wire, forming a fractionally conducting bridge across a broken gold contact, (ii) barrierless quasi-dissociation of a hydrogen molecule occurring upon compression of the contact from the molecular welding configuration, accompanied by switching off of the wire conductance, and (iii) formation of a stable nonconducting gold-hydride wire as a result of the diffusion of hydrogen atoms following the aforementioned quasi-dissociation of the molecule, or as a consequence of diffusion of atomic hydrogen from the tips to the wire region. In addition to the structural and electric transport properties of the bare and hydrogen-adsorbed nanowire configurations, we investigated the dynamical characteristics of the adsorbed hydrogen molecule and have illustrated the sensitivity of the various vibrational modes to the elongation state of the wire.

The various adsorption states of hydrogen to suspended monatomic gold wires revealed by our investigations, and their structural, transport, and dynamical properties, should prove useful for understanding the stability and conductance of atomic gold contacts in a hydrogen atmosphere, and for the interpretation and elucidation of experiments under such conditions. Finally, we note that the reactivity of gold nanowires with hydrogen (in contrast to the well accepted inertness of bulk gold) is consistent with recent findings pertaining to the chemical catalytic activity of gold nanoclusters (in the gas phase and when supported on metal-oxide surfaces), indicating the potential utilization of such nanostructures in nanocatalysis as well as sensor applications.

**Acknowledgment.** This work is supported by the National Science Foundation, the U.S. Air Force Office of Scientific Research, and the U.S. Department of Energy. The computations were performed at the National Energy Supercomputing Center at the Lawrence Berkeley Laboratory, the Army Research Laboratory (ARL-MSRC), and the Georgia tech Center for Computational Materials Science.

## References

- Landman, U.; Luedtke, W. D.; Burnham, W. A.; Colton, R. *J. Science* **1990**, *248*, 454.
- See review in: Agrait, N.; Yeyati, A. L.; van Ruitenbeek, J. M. *Phys. Rep.* **2003**, *377*, 8103.
- Barnett, R. N.; Landman, U. *Nature* **1997**, *387*, 788.
- Ohnishi, H.; Kondo, Y.; Takayanagi, K. *Nature* **1998**, *395*, 780.
- Yanson, A. I.; Rubio Bollinger, G.; van der Brom, H. E.; Agrait, N.; van Ruitenbeek, J. M. *Nature* **1998**, *395*, 783.
- Rodrigues, V.; Ugarte, D. *Phys. Rev. B* **2001**, *63*, 073405.
- Torres, J. A.; Tosatti, E.; Dal Corso, A.; Ercolessi, F.; Kohanoff, J. J.; Di Tolla, F. D.; Soler, J. M. *Surf. Sci.* **1999**, *426*, L441.
- Okamoto, M.; Takayanagi, K. *Phys. Rev. B* **1999**, *60*, 7808.
- Sanchez-Portal, D.; Artacho, E.; Junquera, J.; Ordejon, P.; Carcia, A.; Soler, J. M. *Phys. Rev. Lett.* **1999**, *83*, 3884.
- Häkkinen, H.; Barnett, R. N.; Scherbakov, A.; Landman, U. *J. Phys. Chem. B* **1999**, *103*, 8814.
- De Maria, L.; Springborg, M. *Chem. Phys. Lett.* **2000**, *323*, 293.
- Häkkinen, H.; Barnett, R. N.; Scherbakov, A.; Landman, U. *J. Phys. Chem. B* **2000**, *104*, 9063.
- Sanchez, A.; Abbet, S.; Heiz, A. U.; Schneider, W.-D.; Hakkinen, H.; Barnett, R. N.; Landman, U. *J. Phys. Chem. A* **1999**, *103*, 9573.
- Häkkinen, H.; Abbet, S.; Sanchez, A.; Heiz, U.; Landman, U. *Ang. Chem., Int. Ed.* **2003**, *42*, 1297, and references therein.
- Häkkinen, H.; Moseler, M.; Landman, U. *Phys. Rev. Lett.* **2002**, *89*, 033401.
- Li, C. Z.; Sha, H.; Tao, N. *J. Phys. Rev.* **1998**, *58*, 6775.
- Li, C. Z.; He, X.; Bogozzi, A.; Bunch, J. S.; Tao, N. *J. Appl. Phys. Lett.* **2000**, *76*, 1333.
- Bogozzi, A.; Lam, O.; He, X.; Li, C. Z.; Tao, N. J.; Nagahara, L. A.; Amlani, I.; Tsui, R. *J. Am. Chem. Soc.* **2001**, *123*, 4585.
- Legoas, S. B.; Galvao, D. S.; Rodrigues, V.; Ugarte, D. *Phys. Rev. Lett.* **2002**, *88*, 076195.
- Novaes, F. D.; da Silva, A. D. R.; da Silva, E. Z.; Fazzio, A. *Phys. Rev. Lett.* **2003**, *90*, 036101.
- Skorodumova, N. V.; Simak, S. I. *Phys. Rev. B* **2003**, *67*, 121404.
- (a) Smit, R. H. M.; Noat, Y.; Untiedt, C.; Lang, N. D.; van Hemert, M.; van Ruitenbeek, J. M. *Nature* **2002**, *419*, 906. (b) Smit, R. H. M., Ph.D. Thesis, University of Leiden, The Netherlands, 2003. In these experiments the interaction of a hydrogen molecule with a Pt monatomic-wide nanowire has been studied. In addition to the vibrational frequency with  $h\omega = 64$  meV that is reported in (a) and attributed to shuttle motion of a bridging hydrogen molecule, a frequency above 100 meV is mentioned in (b), see section 4.6, and is attributed to a hindered rotational mode of the molecule. While the conducting electron may couple differently to various vibrational modes, both longitudinal (along the axis of the wire) and transverse modes may be measured. We also note that as stated in (a) high-energy vibrations could not be measured since the contact becomes unstable at bias voltages above 200 meV.
- Csonka, Sz.; Halbritter, A.; Mihaly, G.; Jurdik, E.; Shklyarevskii, O. I.; Speller, S.; van Kempen, H. *Phys. Rev. Lett.* **2003**, *90*, 116803. In these experiments the physical interaction of H<sub>2</sub> condensed on a gold nanowire at 10–30 K has been studied. The lowest peak in the measured conductance histogram at  $G = 0.5 g_0$  is attributed, after ref 10, to hydrogen-assisted stabilization of a gold dimer in a monatomic-wide wire (in ref 10 the conductance of such dimerized bare wire was calculated as 0.58  $g_0$ ; see also Figure 2(iii)). The low temperature in these experiments may make some of the stable configurations in our current investigation inaccessible (particularly those where a chemical rather than a physical interaction occurs), and thus differences between the measured and calculated conductances are to be expected.
- Garcia, Y.; Palacios, J. J.; SanFabian, E.; Verges, A.; Perez-Jimenez, A. J.; Louis, E. *Phys. Rev. B* **2004**, *69*, 41402.
- Barnett, R. N.; Landman, U. *Phys. Rev. B* **1993**, *48*, 2081.
- Perdew, J.; Burk, K.; Ernzerhof, M. *Phys. Rev. Lett.* **1996**, *77*, 3865.
- Troullier, N.; Martins, J. L. *Phys. Rev. B* **1991**, *43*, 1993.
- Hirose, K.; Tsukuda, M. *Phys. Rev. B* **1995**, *51*, 5278.
- For evaluation of the self-consistent potential used in the transfer-matrix calculation, s-local components of the Au and H atoms were used and the Kohn–Sham electronic structure was recalculated.
- Nakamura, A.; Brandbyge, M.; Hansen, L. B.; Jacobsen, K. W. *Phys. Rev. Lett.* **1999**, *82*, 1538.
- Brandbyge, M.; Sorensen, M. R.; Jacobsen, K. W. *Phys. Rev. B* **1997**, *56*, 14956.
- Lian, L.; Hachet, P.; Rayner, D. M. *J. Chem. Phys.* **1993**, *99*, 2.

NL049054N